Microfluidics and Nanofluidics (2018) 22:83
https://doi.org/10.1007/s10404-018-2103-z

RESEARCH PAPER

Numerical investigation of dynamics of elliptical magnetic microparticles in shear flows

Jie Zhang[1] · **Christopher A. Sobecki**[1] · **Yanzhi Zhang**[2] · **Cheng Wang**[1]

Received: 30 May 2018 / Accepted: 19 July 2018 / Published online: 25 July 2018

Abstract

We study the rotational dynamics of magnetic prolate elliptical particles in a simple shear flow subjected to a uniform magnetic field, using direct numerical simulations based on the finite element method. Focusing on paramagnetic and ferromagnetic particles, we investigate the effects of the magnetic field strength and direction on their rotational dynamics. In the weak field regime (below a critical field strength), the particles are able to perform complete rotations, and the symmetry property of particle rotational speed is influenced by the direction and strength of the magnetic field. In the strong field regime (above a critical strength), the particles are pinned at steady angles. The steady angle depends on both the direction and strength of the magnetic field. Our results show that paramagnetic and ferromagnetic particles exhibit markedly different rotational dynamics in a uniform magnetic field. The numerical findings are in good agreement with theoretical prediction. Our numerical investigation further reveals drastically different lateral migration behaviors of paramagnetic and ferromagnetic particles in a wall-bounded simple shear flow under a uniform magnetic field. These two kinds of particles can thus be separated by combining a shear flow and a uniform magnetic field. We also study the lateral migration of paramagnetic and ferromagnetic particles in a pressure-driven flow (a more practical flow configuration in microfluidics), and observe similar lateral migration behaviors. These findings demonstrate a simple but useful way to manipulate non-spherical microparticles in microfluidic devices.

Keywords Microfluidics · Particle separation · Magnetic particles · Rotational dynamics · Lateral migration

1 Introduction

Magnetic particles have been used in a vast number of applications including biomedicine (Pankhurst et al. 2003), biological analysis, and chemical catalysis (Gijs et al. 2009; Pamme 2012). The separation of magnetic microparticles and nanoparticles in microscale fluid environments is one of the most important processes in the systems and platforms based on microfluidic technology (Pamme 2006, 2012). A magnetic field is a powerful tool to separate magnetic particles or magnetically labelled cells, antigens, and enzymes (Gijs 2004; Pamme 2006; Suwa and Watarai 2011). Most magnetic separation methods are based on magnetophoresis, which manipulates magnetic particles in a viscous fluid using magnetic forces. To generate the magnetic force, it requires both magnetic particles and a spatially nonuniform field (magnetic field gradient) (Pamme 2006). There are two different types of magnetophoresis: one is called negative magnetophoresis— manipulating diamagnetic particles in a magnetic fluid such as ferrofluids (Winkleman et al. 2007; Bucak et al. 2011; Zhou et al. 2016; Zhou and Xuan 2016); the other one is called positive magnetophoresis—separating paramagnetic or ferromagnetic particles in a non-magnetic fluid such as water (Zborowski et al. 1999; Chen et al. 2015).

In contrast to conventional magnetophoresis, several recent experimental, numerical, and theoretical studies Zhou et al. (2017a, b), Matsunaga et al. (2017a, b), Cao et al. (2018) and Zhang and Wang (2018) have demonstrated a different way to manipulate magnetic non-spherical particles by a uniform magnetic field in

✉ Cheng Wang
wancheng@mst.edu

[1] Department of Mechanical and Aerospace Engineering, Missouri University of Science and Technology, 400 W. 13th St., Rolla, MO 65409, USA

[2] Department of Mathematics and Statistics, Missouri University of Science and Technology, 400 W. 12th St., Rolla, MO 65409, USA

the microchannel. The uniform magnetic field does not generate a magnetic force, but instead generates non-zero magnetic torques due to the non-spherical particle shape. When coupled with particle–wall hydrodynamic interaction (Gavze and Shapiro 1997; Leal 1980), the uniform magnetic field alters the rotational dynamics of non-spherical particles, and consequently controls the lateral migration of particles. Experiments performed by Zhou et al. (2017a, b) have demonstrated that a weak uniform magnetic field can separate paramagnetic particles in a microchannel pressure-driven flow. The magnetic torque broke the symmetry of the particle rotation. Due to the particle–wall hydrodynamic interaction, the particles migrated laterally towards or away from the wall depending on the direction of magnetic field. Using the finite element method (FEM), Cao et al. (2018) and Zhang and Wang (2018) investigated the effect of several parameters, such as the strength and direction of the magnetic field, particle aspect ratio, and flow rate, on the lateral migration of the paramagnetic particles in microchannels. In another study, Matsunaga et al. (2017a, b) proposed a far-field theory and used the boundary element method to demonstrate that a strong uniform magnetic field can separate the ferromagnetic particles in both simple shear flow near the wall and Poiseuille flow between two walls. In this method, ferromagnetic particles are pinned at steady angles and the lateral migration results from particle–wall hydrodynamic interactions as well.

Previous investigations have either studied the lateral migration of paramagnetic particles under a weak magnetic field (Zhou et al. 2017a, b; Cao et al. 2018; Zhang and Wang 2018) or ferromagnetic particles under a strong magnetic field (Matsunaga et al. 2017a, b). A comprehensive understanding on the difference of the lateral migration mechanism between the paramagnetic and ferromagnetic particles under both the weak and strong magnetic fields is absent. In our previous theoretical work Sobecki et al. (2018), we theoretically analyzed the difference of particle rotational dynamics between the paramagnetic and ferromagnetic particles in a simple shear flow under a magnetic field. However, due to the inherent complexity of particle dynamics in bounded flows, systematic theoretical analysis is difficult. In this work, we systematically investigate the rotational dynamics of both paramagnetic and ferromagnetic elliptical particles under a uniform magnetic field in simple shear and bounded flows using direct numerical simulations. Our results suggest that the difference in magnetic properties leads to markedly different rotational dynamics as well as lateral migration. Based on these insights, we demonstrate feasible ways to separate these two kinds of magnetic particles in a pressure-driven flow configuration, which are commonly used in practical applications such as microfluidic devices.

This paper is organized as follows. Section 2 presents the numerical method including mathematical modeling, material parameters used in the simulation, and validation of the numerical method. Section 3 presents a brief theoretical analysis for comparing the numerical and theoretical results in following sections. Sections 4 and 5 numerically investigate the rotational dynamics of paramagnetic and ferromagnetic particles in a simple shear flow under weak and strong magnetic fields, and compare the numerical and theoretical results. Based on the discussion in Sects. 4 and 5, 6 studies the lateral migration of paramagnetic and ferromagnetic particles in a simple shear flow near the wall. Finally, in Sect. 7, the simulation for the lateral migration of paramagnetic and ferromagnetic particles in a microchannel pressure-driven flow under both a weak and strong magnetic fields is preformed to demonstrate particle separation in more practical flows.

2 Numerical method

2.1 Mathematical model

We consider a rigid prolate elliptical particle suspended in a simple shear flow as shown in Fig. 1. The computational domain, Ω, is bounded by the boundary, ABCD, and

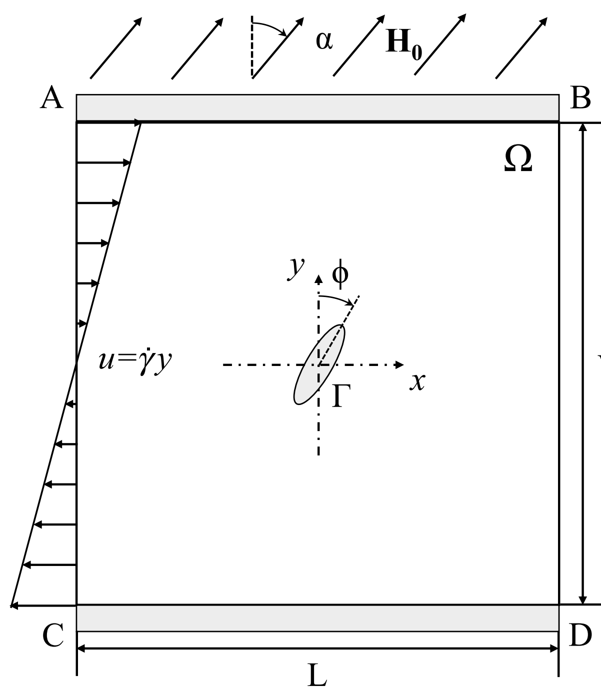

Fig. 1 Schematic of the numerical model of an elliptical particle suspended in a simple shear flow under a uniform magnetic field $\mathbf{H}_0$. The fluid domain and particle surface are Ω and Γ, respectively. The orientation angle of the particle is denoted by ϕ

particle surface, Γ. The width and length of the computational domain are W and L, respectively. The center of the particle is set to be the center of the computational domain. The particle aspect ratio is $r_{\mathrm{p}} = a/b$, where a and b are the major and minor semi-axis lengths of particles, respectively. The orientation angle of the particle, ϕ, is the angle between the major axis of the particle and the positive y axis. The background flow is a simple shear flow, where the velocity $\mathbf{u}_{\infty} = \dot{\gamma} y \mathbf{e}_x$ is imposed, with $\dot{\gamma}$ being the shear rate. A uniform magnetic field, $\mathbf{H}_0$, is applied at an arbitrary direction, denoted by α.

The fluid is assumed to be incompressible, Newtonian, and non-magnetic. The transient flow field is governed by the continuity equation and Navier–Stokes equation:

$$\nabla \cdot \mathbf{u} = 0, \tag{1}$$

$$\rho_f \left[\frac{\partial \mathbf{u}}{\partial t} + (\mathbf{u} \cdot \nabla)\mathbf{u} \right] = -\nabla p + \nabla \cdot \eta_f \left(\nabla \mathbf{u} + (\nabla \mathbf{u})^T\right), \tag{2}$$

where $\mathbf{u}$ is the velocity vector, ρ_f and η_f are the density and dynamic viscosity of the fluid, respectively, p is the pressure, and t is the time.

To impose simple shear, the velocities at the top (AB) and bottom (CD) walls are set to be $\pm\frac{1}{2}\dot{\gamma} W \mathbf{e}_x$ respectively. The boundaries AC and BD are set to periodic flow conditions. With the no-slip condition applied on the particle surface, the fluid velocities on the particle surface Γ are expressed as

$$\mathbf{u} = \mathbf{U}_p + \boldsymbol{\omega}_p \times (\mathbf{x}_s - \mathbf{x}_p), \tag{3}$$

where $\mathbf{U}_p$ and $\boldsymbol{\omega}_p$ are the translational and rotational velocities of particle, respectively, $\mathbf{x}_s$ and $\mathbf{x}_p$ are the position vectors of the surface and the center of the particle. The hydrodynamic force and torque acting on the particle are

$$\mathbf{F}_h = \int (\boldsymbol{\tau}_h \cdot \mathbf{n}) d\Gamma, \tag{4}$$

$$\mathbf{L}_h = \int (\boldsymbol{\tau}_h \times (\mathbf{x}_s - \mathbf{x}_p) \cdot \mathbf{n}) d\Gamma, \tag{5}$$

where $\boldsymbol{\tau}_h = \eta_f \left(\nabla \mathbf{u} + (\nabla \mathbf{u})^T\right)$ is the hydrodynamic stress tensor on the particle surface Γ.

The magnetic field is governed by the static Maxwell equations:

$$\nabla \times \mathbf{H} = 0, \tag{6}$$

$$\nabla \cdot \mathbf{B} = 0, \tag{7}$$

where $\mathbf{H}$ and $\mathbf{B}$ are the magnetic field and the magnetic flux density, respectively. To impose a uniform magnetic field, a magnetic scalar potential difference is set across boundaries AB and CD, with a zero magnetic potential $V_m = 0$ on AB and a magnetic potential $V_m = V_{m0}$ on CD. Magnetic insulation condition is applied on boundaries AC and BD.

Assuming that the particle is homogeneous and isotropic in magnetic properties, the magnetic force acting on the particle, due to a uniform magnetic field, is zero (Stratton 2007). The magnetic torque acting on a magnetic particle is expressed as (Stratton 2007)

$$\mathbf{L}_m = \mu_0 (\mathbf{m} \times \mathbf{H}_0), \tag{8}$$

where $\mathbf{m}$ is the magnetic moment of the particle, and μ_0 is the magnetic permeability of the vacuum.

For two-dimensional elliptical particles, the rotational motion is in the x–y plane, thus $\boldsymbol{\omega}_p = \omega_p \mathbf{e}_z$, $\mathbf{L}_h = L_h \mathbf{e}_z$, and $\mathbf{L}_m = L_m \mathbf{e}_z$. The translation and rotation of particles are governed by Newton's second law and Euler's equation:

$$m_p \frac{d\mathbf{U}_p}{\mathrm{d}t} = \mathbf{F}_h, \tag{9}$$

$$I_p \frac{d\omega_p}{\mathrm{d}t} = L_h + L_m, \tag{10}$$

where m_p and I_p are the mass and the moment of inertia of the particle, respectively.

The position of the particle center $\mathbf{x}_p(t) = (x_p, y_p)$ and the orientation ϕ of the particle are expressed as

$$\mathbf{x}_p(t) = \mathbf{x}_p(0) + \int_0^t \mathbf{U}_p(t')\mathrm{d}t', \tag{11}$$

$$\phi(t) = \phi(0) + \int_0^t \omega_p(t')\mathrm{d}t', \tag{12}$$

where $\mathbf{x}_p(0)$ and $\phi(0)$ are the initial position and orientation of the particle.

The dynamic motions of the particle, the flow field, and the magnetic field are coupled via Eqs. (3–5) and (8–10). We use direct numerical simulation (DNS) based on FEM and arbitrary Lagrangian–Eulerian(ALE) method to simultaneously calculate the flow field and particle motion. Similar methodologies have been successfully used by Hu et al. (2001), Ai et al. (2009a, b, 2014) and Ai and Qian (2010). The numerical model is implemented and solved with a commercial FEM solver (COMSOL Multiphysics). First, we use a stationary solver to calculate the magnetic field inside and outside of the particle and compute the magnetic torque acting on the particle. Then, the two-way coupling of fluid-particle interaction model is solved using a time-dependent solver and by importing the previously determined magnetic torque. The deformation of the computational domain is solved with the moving mesh interface based on the ALE algorithm. The meshes of fluid domain are free to deform, while the particle domain is determined by its trajectory and orientation. As the mesh deforms, the mesh quality is decreased. When the quality value is decreased to 0.2, the re-meshing process initiates. Similar modeling strategy has been successfully carried out in our previous work (Zhang and Wang 2018) and other work, e.g., Cao et al. (2018). Quadratic triangular elements are employed in this simulation. A fine mesh around the particle and a finer mesh around the tip of the particle are created to accurately calculate the hydrodynamic force and torque acting on the particle. The total number of elements was about 7000 in the fluid domain Ω, and about 130 elements were used to discretize the particle surface Γ.

2.2 Material properties

In this numerical study, water is used as the nonmagnetic fluid ($\chi_f = 0$), which has a density $\rho_f = 1000$ kg/m^3 and a dynamic viscosity $\eta_f = 1 \times 10^{-3}$ Pa s. The shear rate of the flow is kept constant, such that $\dot{\gamma} = 200$ s^{-1}. The particle is assumed to be polystyrene particles containing magnetic nanoparticles, similar to those used in earlier experiments (Zhou et al. 2017a, b), which could be either paramagnetic or ferromagnetic particles. The density of the particle is $\rho_p = 1100$ kg/m^3. Here, the particle motion is in the x–y plane and the inertia effect is negligible, thus the density difference between the particle and fluid has negligible effect on the particle dynamics. The equivalent diameter of the particle used in this simulation is $d = 7\ \mu$m and the particle aspect ratio $r_p = 4$, thus the major and minor semi-axis lengths of particles are $a = 7\mu$m and $b = 1.75\mu$m. We consider two kinds of magnetic particles: paramagnetic particles with $\chi_p = 0.26$ and ferromagnetic particle with permanent magnetization $\boldsymbol{M}_0 = 2000$ A/m.

2.3 Validation of numerical method

In this section, we present validation of the numerical method by comparing the results with Jeffery's theory, which describes the periodic rotation of an axisymmetric ellipsoidal particle in a simple shear unbounded flow (Jeffery 1922). Without a magnetic field, the ferromagnetic and paramagnetic particles behave the same way. Here, the width and length of the computational domain are W = L = 150 μm, which will also be used in the simulations in Sects. 4 and 5. The confinement effects of the walls are negligible due to the large computational domain relative to the particle size. The period of the particle rotation, T^J, is defined as the time taken by the particle to rotate from $\phi = 0$ to $\phi = 360°$, and $T^J = 2\pi/\dot{\gamma}(r_p + 1/r_p)$ (Jeffery 1922). Due to the fore–aft symmetry of the particle, we define T_0^J as the time taken for rotation from 0 to 180°, i.e., $T_0^J = T^J/2$. Note that for ease of visualizing results, we use both 'degree' and 'radian' as units for angles in the remaining sections of this paper.

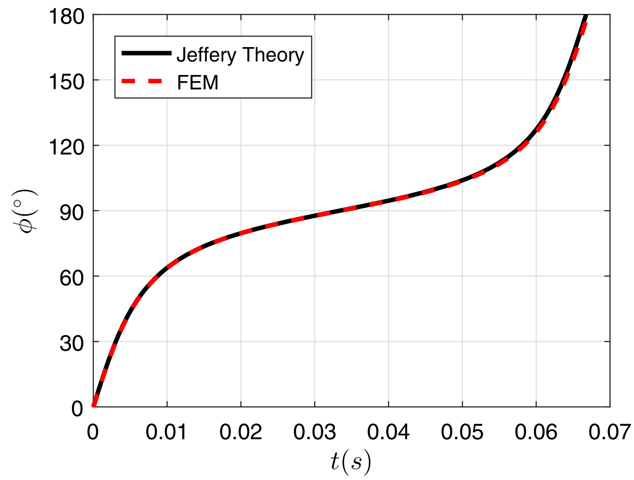

Fig. 2 Comparison between the FEM simulation and Jeffery's theory for particle aspect ratio $r_p = 4$ and the shear rate $\dot{\gamma} = 200$ s^{-1}

Table 1 Four meshes for grid independence analysis

	Domain elements	Boundary elements on particle surface
Mesh 1	3734	48
Mesh 2	4812	76
Mesh 3	6952	124
Mesh 4	7548	148

Figure 2 compares the time evolution of particle orientation angle predicted by Jeffery's theory and our simulation for a particle with $r_p = 4$ in a simple shear flow ($\dot{\gamma} = 200$ s $^{-1}$). The theoretical value of T_0^J from Jeffery's theory is 0.0668 s, while the period obtained in our FEM simulation is 0.0670 s. The relative error is 0.3%, suggesting that the simulation has excellent agreement with the theory. Therefore, this simulation method has been validated to be sufficiently accurate to study the dynamics of the particle in a simple shear flow.

2.4 Grid independence analysis

We perform grid independence analysis to determine the appropriate meshes for cost-effective numerical simulations without comprising accuracy. The results for four different meshes in a simple shear flow in the absence of the magnetic field are shown in Table 1 and Fig. 3. As can be seen, the convergence of numerical results is considered sufficient when the domain element number is larger than 6,952 and the boundary element number on the particle surface is larger than 124. In this work, we use about 7500 elements in the computational

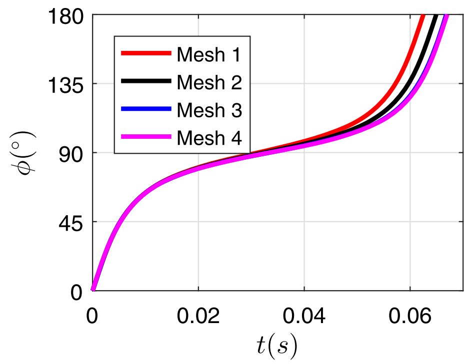

Fig. 3 Grid independence analysis: particle orientation ϕ as a function of time t for particle aspect ratio $r_p = 4$ and the shear rate $\dot{\gamma} = 200$ s^{-1}

domain Ω in Fig. 1, and about 150 elements on the particle surface Γ, which give reasonably accurate results.

3 Theoretical analysis

In this section, we briefly present the theoretical analysis pertaining to the rotational dynamics of paramagnetic and ferromagnetic particles. We also define relevant dimensionless parameters as well as physical quantities to characterize the rotational behaviors.

Assuming a small particle Reynolds number, (i.e., $\mathrm{Re}_p = \rho_p d^2 \dot{\gamma}/\eta_f \ll 1$, justified by typical microfluidic experimental conditions), the particle inertia is negligible and the particle motion is quasi-steady, similar to the previous studies (Allan and Mason 1962; Chaffey and Mason 1964; Okagawa et al. 1974). Equation (10) is then reduced to

$$L_h + L_m = 0. \tag{13}$$

Under the assumption of Stokes flow, the hydrodynamic torque in the xy plane acting on an ellipsoidal particle in a simple shear flow with a shear rate $\dot{\gamma}$ is (Jeffery 1922; Okagawa et al. 1974)

$$L_h = \frac{8\pi\eta_f a^3(r_p^2+1)}{3r_p^2(D_{xx}+D_{yy})}\left(\frac{r_p^2-1}{r_p^2+1}\frac{\cos(2\phi)}{2}\dot{\gamma}+\frac{\dot{\gamma}}{2}-\omega_p\right), \tag{14}$$

where $\omega_p = d\phi/\mathrm{d}t$ is the particle rotational speed, $D_{xx} = 1 - A$ and $D_{yy} = A/2$ are the ellipsoidal demagnetizing factors, and $A = \frac{r_p^2}{r_p^2-1} - \frac{r_p\cos^{-1}(r_p)}{(r_p^2-1)^{3/2}}$ for a prolate ellipsoid (Okagawa et al. 1974). When the magnetic field is absent, we obtain the rotational speed due to the hydrodynamic torque only:

$$\omega_h = \frac{r_p^2\cos(\phi)^2+\sin^2(\phi)}{r_p^2+1}\dot{\gamma}, \tag{15}$$

which is the Jeffery equation.

When subjected to an external magnetic field, a magnetic moment is induced in a *paramagnetic* particle, thus resulting in a magnetic torque. According to previous works (Shine and Armstrong 1987; Zhou et al. 2017a, b), the torque experienced by the paramagnetic particle is

$$L_{mp} = -V_p\frac{\mu_0\chi_p^2H_0^2(D_{yy}-D_{xx})\sin(2(\phi-\alpha))}{2(\chi_pD_{xx}+1)(\chi_pD_{yy}+1)}, \tag{16}$$

where V_p is the volume of the particle. Substituting Eqs. (14) and (16) into Eq. (13), the total particle rotational speed is obtained:

$$\omega_p = \frac{d\phi}{\mathrm{d}t} = \frac{r_p^2\cos(\phi)^2+\sin^2(\phi)-S_p\sin(2(\phi-\alpha))}{r_p^2+1}\dot{\gamma}, \tag{17}$$

where

$$S_p = \frac{\mu_0\chi_p^2H_0^2(r_p^2D_{xx}+D_{yy})(D_{yy}-D_{xx})}{4\dot{\gamma}\eta_f(1+\chi_pD_{xx})(1+\chi_pD_{yy})}. \tag{18}$$

The dimensionless parameter S_p measures the relative strength between the magnetic and hydrodynamic effects on a paramagnetic particle (Zhou et al. 2017a, b).

For a *ferromagnetic* particle, it is assumed that the magnetization of the particle, $\mathbf{M_0}$ (its magnitude denoted by M_0) is parallel to the particle's major axis. The magnetic moment of the particle $\mathbf{m} = V_p\mathbf{M_0} = V_pM_0(\sin(\phi), \cos(\phi), 0)$. Thus, Eq. (8) can be written as $\mathbf{L}_{mf} = \mu_0V_p(\mathbf{M}_0\times\mathbf{H}_0) = L_{mf}\mathbf{e}_z$, with the magnitude of the torque (Shine and Armstrong 1987)

$$L_{mf} = -\mu_0V_pM_0H_0\sin(\phi-\alpha). \tag{19}$$

We obtain the total rotational speed of a ferromagnetic particle in a simple shear flow (Sobecki et al. 2018):

$$\omega_p = \frac{d\phi}{\mathrm{d}t} = \frac{r_p^2\cos(\phi)^2+\sin^2(\phi)-S_f\sin(\phi-\alpha)}{r_p^2+1}\dot{\gamma}, \tag{20}$$

where

$$S_f = \frac{\mu_0M_0H_0(r_p^2D_{xx}+D_{yy})}{2\eta_f\dot{\gamma}} \tag{21}$$

is a dimensionless parameter that measures the relative strength between the magnetic and hydrodynamic effects on a ferromagnetic particle.

As can be seen in Eqs. (17) and (20), the particle rotational behaviour depends on the direction of magnetic field α and the parameters S_p or S_f. When S_p or S_f is increased to a large enough value, the particle rotation is impeded. In our previous work (Zhou et al. 2017b), we defined S_{cr} as the critical value of S for the existence of real solutions to $\omega_p = 0$. When $S \geq S_{cr}$, the particle is impeded at a certain steady angle ϕ_s, and we define this field as the strong magnetic field. When $S < S_{cr}$, the particle is able to perform full rotations, so we define this field as the weak magnetic field. For simplicity of notation, in the following sections, we use S to represent either S_p for paramagnetic particles or S_f for ferromagnetic particles.

The critical relative strength, S_{cr}, can be calculated from Eq. (17) for paramagnetic particles and Eq. (20) for ferromagnetic particles. The values of S_{cr} for $r_p = 4$ are shown in Table 2 for various magnetic field directions (α) (Sobecki et al. 2018).

In the weak field regime, to better compare the difference between paramagnetic and ferromagnetic particles, we define the period of rotation as the time taken by the particle to rotate from 0 to 2π (or 360°) as $T = T_1 + T_2$ with

$$T = \int_0^{2\pi} \frac{d\phi}{\omega_p}, \qquad T_1 = \int_0^{\pi} \frac{d\phi}{\omega_p}, \qquad T_2 = \int_{\pi}^{2\pi} \frac{d\phi}{\omega_p}. \tag{22}$$

In our previous work (Zhou et al. 2017b), due to π(180°) period of the paramagnetic particle, we defined a ratio parameter

$$\tau_1 = \int_0^{\pi/2} \frac{d\phi}{\omega_p} \Big/ \int_0^{\pi} \frac{d\phi}{\omega_p} \tag{23}$$

to characterize the symmetry property of the paramagnetic particle rotation. However, the ferromagnetic particle rotates periodically with a period of 2π (or 360°), thus we define an additional ratio parameter

$$\tau_2 = \int_{\pi}^{3\pi/2} \frac{d\phi}{\omega_p} \Big/ \int_{\pi}^{2\pi} \frac{d\phi}{\omega_p} \tag{24}$$

We use the average of τ_1 and τ_2 as τ to characterize the overall symmetry property of the particle rotation, that is,

$$\tau = \frac{\tau_1 + \tau_2}{2}. \tag{25}$$

As can be seen, for the paramagnetic particle, $\tau_1 = \tau_2 = \tau$.

In the following sections, we will investigate the difference of rotational dynamics between paramagnetic and ferromagnetic particles using systematic numerical simulations under both weak and strong magnetic fields. Specifically, we will study the effect of magnetic field on the period of rotation, symmetry properties of the particle rotation, and impeded angles. In addition, the numerical and theoretical results are compared and discussed.

4 Weak magnetic field

We will focus on the rotational dynamics of paramagnetic and ferromagnetic particles in the presence of a weak magnetic field ($S < S_{cr}$). In this regime, both particles are able to perform complete rotations. However, the magnetic field will affect their rotation differently because the the magnetic torques have different dependence on the parameter $(\phi - \alpha)$ as in Eqs. (16) and (19).

4.1 Paramagnetic particles

First, we discuss the rotational dynamics of paramagnetic particle in a weak magnetic field. The rotational motion of the paramagnetic magnetic particle with $r_p = 4$ when the magnetic field is applied perpendicular to the flow direction ($\alpha = 0°$) is shown in Fig. 4. Figure 4a shows the time evolution of orientation angle of the particle, ϕ, with time t when the relative strength S is increased from 0 to 5.04. As can be seen, the period of rotation increases with an increasing S. With $S \approx 5.04$, the particle is impeded at a steady angle $\phi_s = 61.56°$. The numerical results are in quantitative agreement with the prediction ($S_{cr} = 4$) from our previous theory (Zhou et al. 2017b). We study the dimensionless parameters τ_1 and τ_2 in Fig. 4b, c. The numerical results show that $\tau_1 = \tau_2 = \tau$ for the paramagnetic particle, independent of the magnetic strength $S < S_{cr}$, which is consistent with the theoretical results in Sect. 3. Thus, we only discuss τ in the remaining of this section.

The effect of the magnetic field on the period of rotation is shown in Fig. 5. To better illustrate this effect, the dimensionless period is defined by normalizing T with the Jeffery period T^J. We investigate four different directions of the magnetic field. At each direction, the dimensionless period changing with magnetic field strength S is studied. The symbols represent the numerical results and the solid lines are the theoretical predictions from Eq. (22). We observe that the dimensionless

Table 2 The critical strength, S_{cr}, calculated for paramagnetic and ferromagnetic particles with $r_p = 4$, and different α Sobecki et al. (2018)

α(°)	0	45	90	135	180	225	270	315
Paramagnetic	4	1	4	16	4	1	4	16
Ferromagnetic	1	1.38	7.75	1.38	1	1.38	7.75	1.38

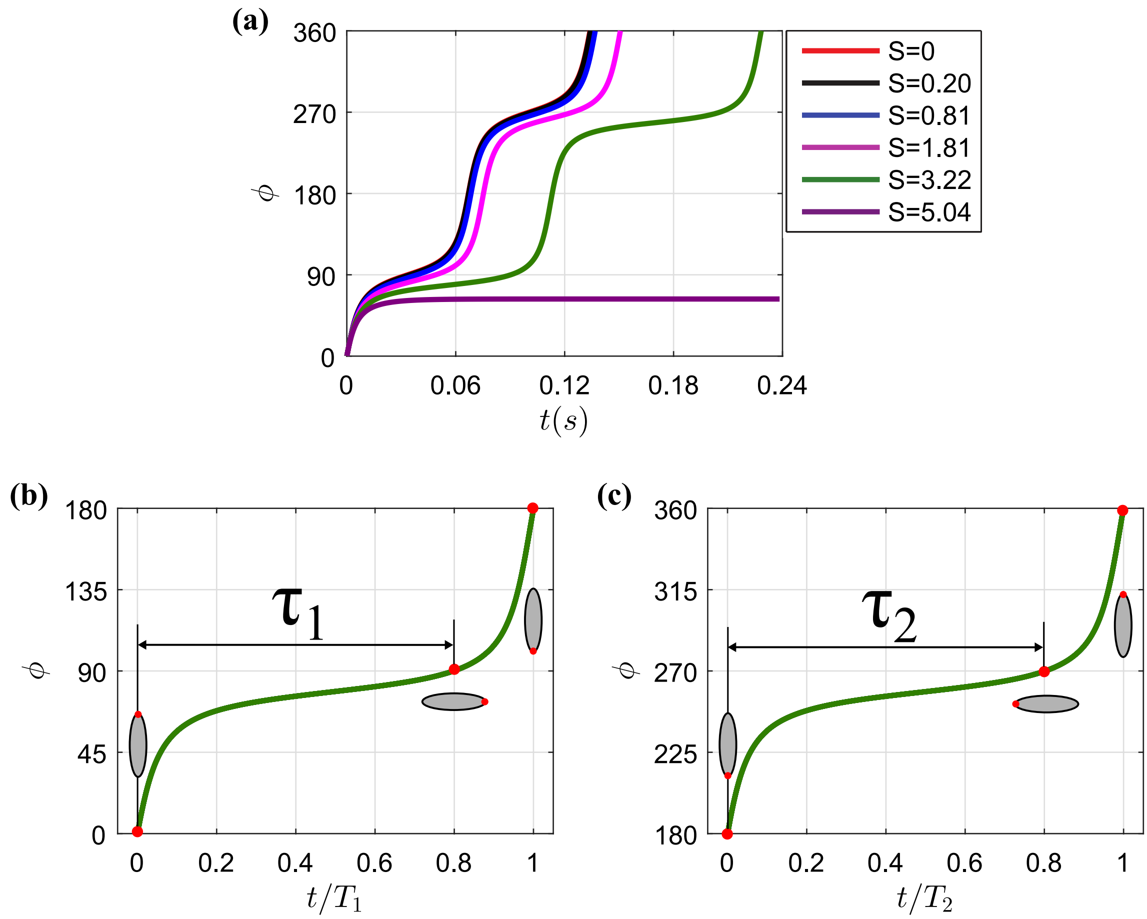

Fig. 4 Rotation of the paramagnetic magnetic particle ($r_p = 4$) when the magnetic field is applied perpendicular to the flow direction ($\alpha = 0°$). **a** The times evolution of orientation angle, ϕ; **b** The evolution of orientation angle, ϕ, with the dimensionless time, t/T_1; **c** The evolution of orientation angle, ϕ, with the dimensionless time, t/T_2. T_1 and T_2 denote times taken by the particle to rotate from 0° to 180° and from 180° to 360°, respectively

period, T/T^J, increases monotonically with an increase of S when the magnetic field is applied at $\alpha = 0°$(a), $\alpha = 45°$(b), and $\alpha = 90°$(c). When the magnetic field is applied at $\alpha = 135°$ (d), the dimensionless period, T/T^J, decreases first, and then increases. Furthermore, these numerical results are in quantitative agreement with those when the paramagnetic particle is transported in a pressure-driven flow Zhang and Wang (2018). Additionally, the numerical results are in a very good agreement with the theoretical prediction.

Figure 6 shows the dimensionless parameter, τ, as a function of S when the magnetic field is applied at $\alpha = 0°$, $\alpha = 45°$, $\alpha = 90°$ and $\alpha = 135°$. When the field is applied at $\alpha = 0°$ and 90°, as can be seen in Fig. 6a, c, τ deviates further from 0.5 as S is increased, meaning the asymmetry of the particle rotation becomes more pronounced. Interestingly, when the magnetic field is applied at $\alpha = 45°$ and 135° as can be seen in Fig. 6b, d, τ is always equal to 0.5, independent of the strength S, meaning the particle rotation is always symmetric with respect to $\phi = 90°$ and 270°. The numerical simulation results have a remarkable agreement with the theoretical results.

4.2 Ferromagnetic particles

We now look at the rotational dynamics of a ferromagnetic particle under the weak magnetic field regime. Because the rotation of ferromagnetic particle has a period of 2π (or 360°) in ϕ, we perform simulations with the magnetic field applied at $\alpha = 0°$, 45°, 90°, 135°, 180°, 225°, 270° and 315°. Figure 7 shows the dimensionless period, T/T^J, changing with the dimensionless magnetic field strength, S, when the magnetic field is applied at these eight angles. As we can see, the dimensionless period of rotation, T/T^J, increases monotonically with an increase of S at all directions of the magnetic field, which is different from the phenomena observed in Fig. 6 for paramagnetic particles. When the magnetic field is applied at 135°, T/T^J is decreased first and then increased monotonically

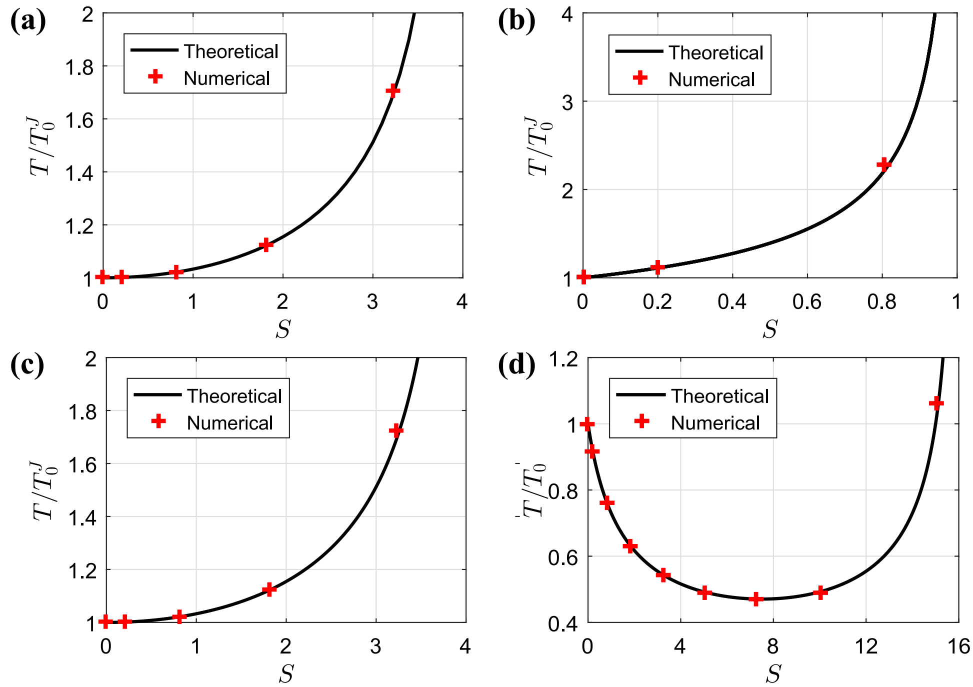

Fig. 5 The dimensionless period, T/T^J, varies with the dimensionless magnetic field strength, S, when the magnetic field is applied at $\alpha = 0°$ (**a**), $\alpha = 45°$ (**b**), $\alpha = 90°$ (**c**) and $\alpha = 135°$ (**d**) for the paramagnetic particle

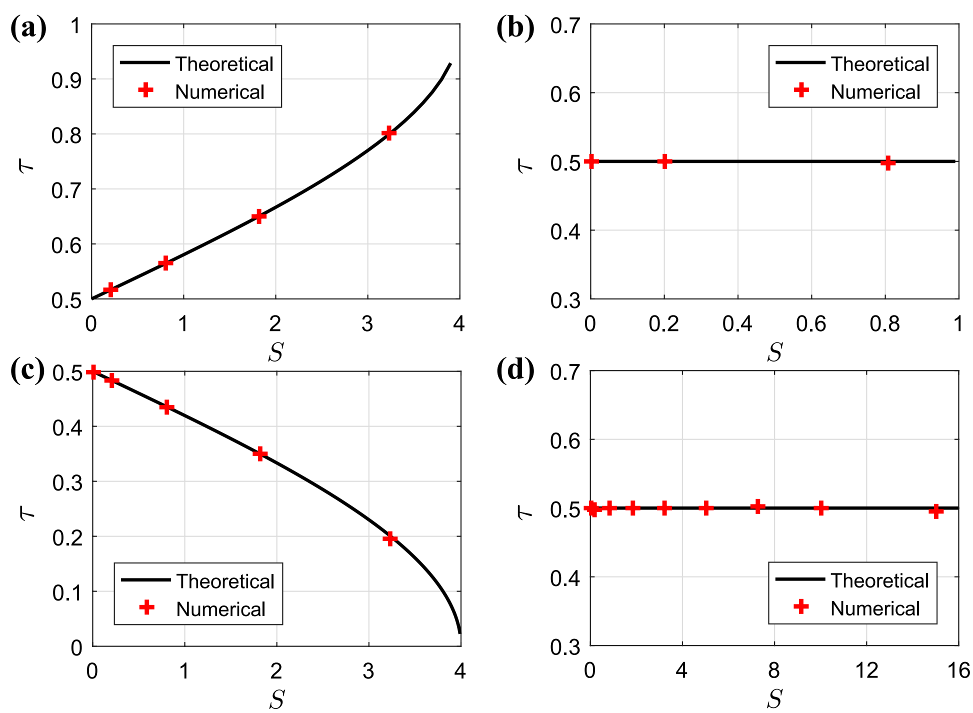

Fig. 6 The dimensionless parameter, τ, varies with the dimensionless magnetic field strength, S, when the magnetic field is applied at $\alpha = 0°$ (**a**), $\alpha = 45°$ (**b**), $\alpha = 90°$ (**c**) and $\alpha = 135°$ (**d**) for the paramagnetic particle

with increasing S for a paramagnetic particle, but for a ferromagnetic particle, T/T^J is increased with increasing S. The numerical simulation results show remarkable agreement with the theoretical results.

The dimensionless parameter, τ, depends on the direction of the magnetic field, α, and field strength, S, as shown in Fig. 8. As can be seen from Fig. 8a, e, when the magnetic field is applied at $\alpha = 0°$ and $180°$, $\tau_1 = \tau_2 = \tau = 0.5$ as S is increased, which is different from the paramagnetic particle in Sect. 4.1 where $\tau_1 = \tau_2 = \tau > 0.5$ and increases with increasing S. Note that paramagnetic particles behave the same when the magnetic field is applied at $\alpha = 180°$ and $\alpha = 0°$. When the magnetic field is applied at $\alpha = 90°$ as shown in Fig. 8c, $\tau_1 < 0.5$, $\tau_2 > 0.5$, and both deviate

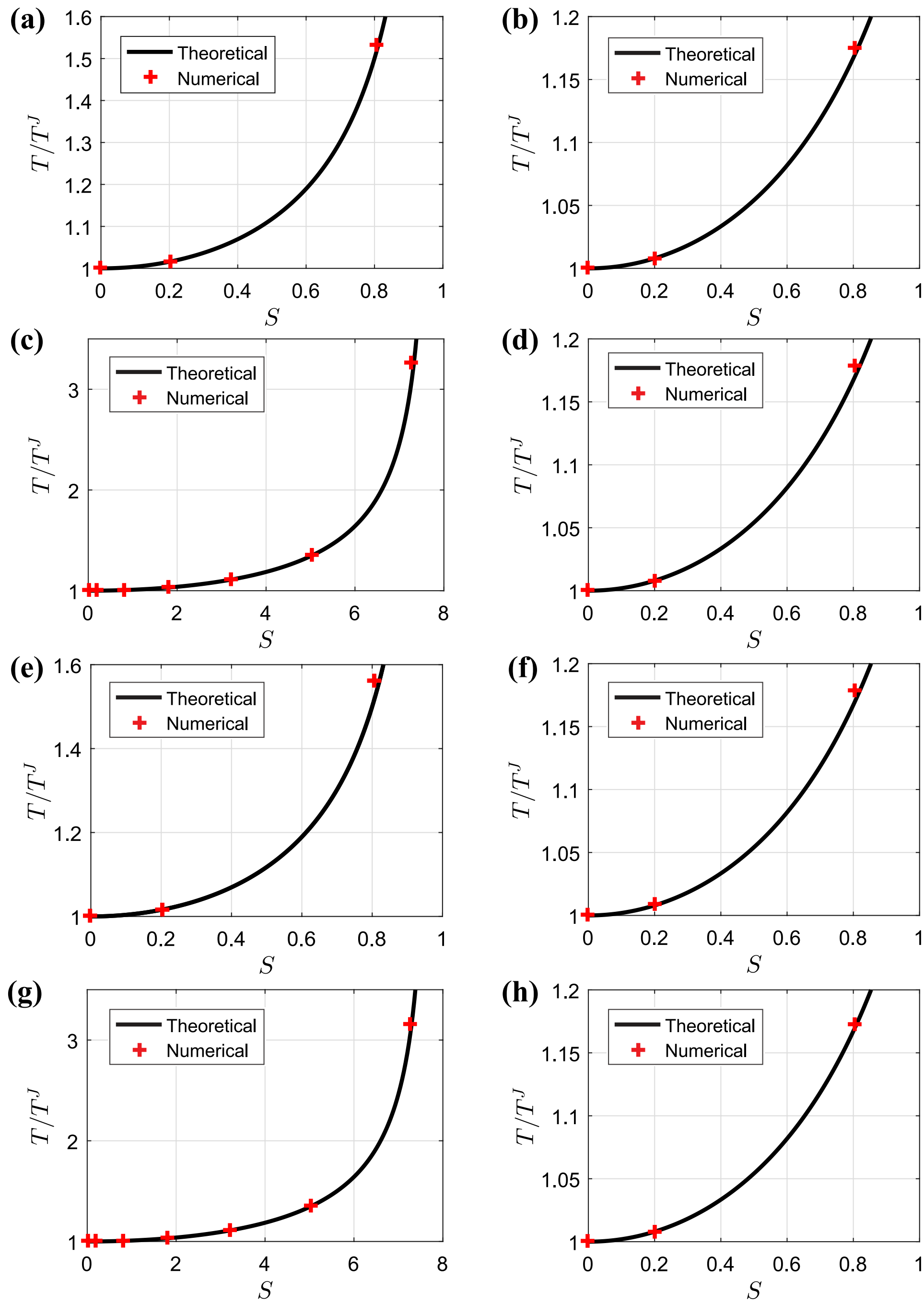

Fig. 7 The dimensionless period, T/T^J, varies with the dimensionless magnetic field strength, S, when the magnetic field is applied at $\alpha = 0°$ (**a**), $\alpha = 45°$ (**b**), $\alpha = 90°$ (**c**), $\alpha = 135°$ (**d**), $\alpha = 180°$ (**e**), $\alpha = 225°$ (**f**), $\alpha = 270°$ (**g**) and $\alpha = 315°$ (**h**) for the ferromagnetic particle

more from 0.5 with increasing S, but τ remains 0.5. Similar results are observed when the magnetic field is applied at $\alpha = 270°$ as shown in Fig. 8g. In this case, $\tau_1 > 0.5$, $\tau_2 < 0.5$, and $\tau = 0.5$ for all values of S. These results are different from the paramagnetic particle in Sect. 4.1 where $\tau_1 = \tau_2 = \tau < 0.5$ and are decreased with increasing S.

When the magnetic field is applied at $\alpha = 45°$, $\tau_1 < 0.5$, $\tau_2 > 0.5$, and $\tau < 0.5$; when the magnetic field is applied at $\alpha = 135°$, $\tau_1 < 0.5$, $\tau_2 > 0.5$, but $\tau > 0.5$; when the magnetic field is applied at $\alpha = 225°$, $\tau_1 > 0.5$, $\tau_2 < 0.5$, and $\tau < 0.5$; when the magnetic field is applied at $\alpha = 315°$, $\tau_1 > 0.5$, $\tau_2 < 0.5$, but $\tau > 0.5$. These three parameters deviate further away from 0.5 with increasing S when the magnetic field is applied at $\alpha = 45°$, 135°, 225° and 315°, which are different from the paramagnetic particle in Sect. 4.1, where $\tau_1 = \tau_2 = \tau = 0.5$ in the weak field regime.

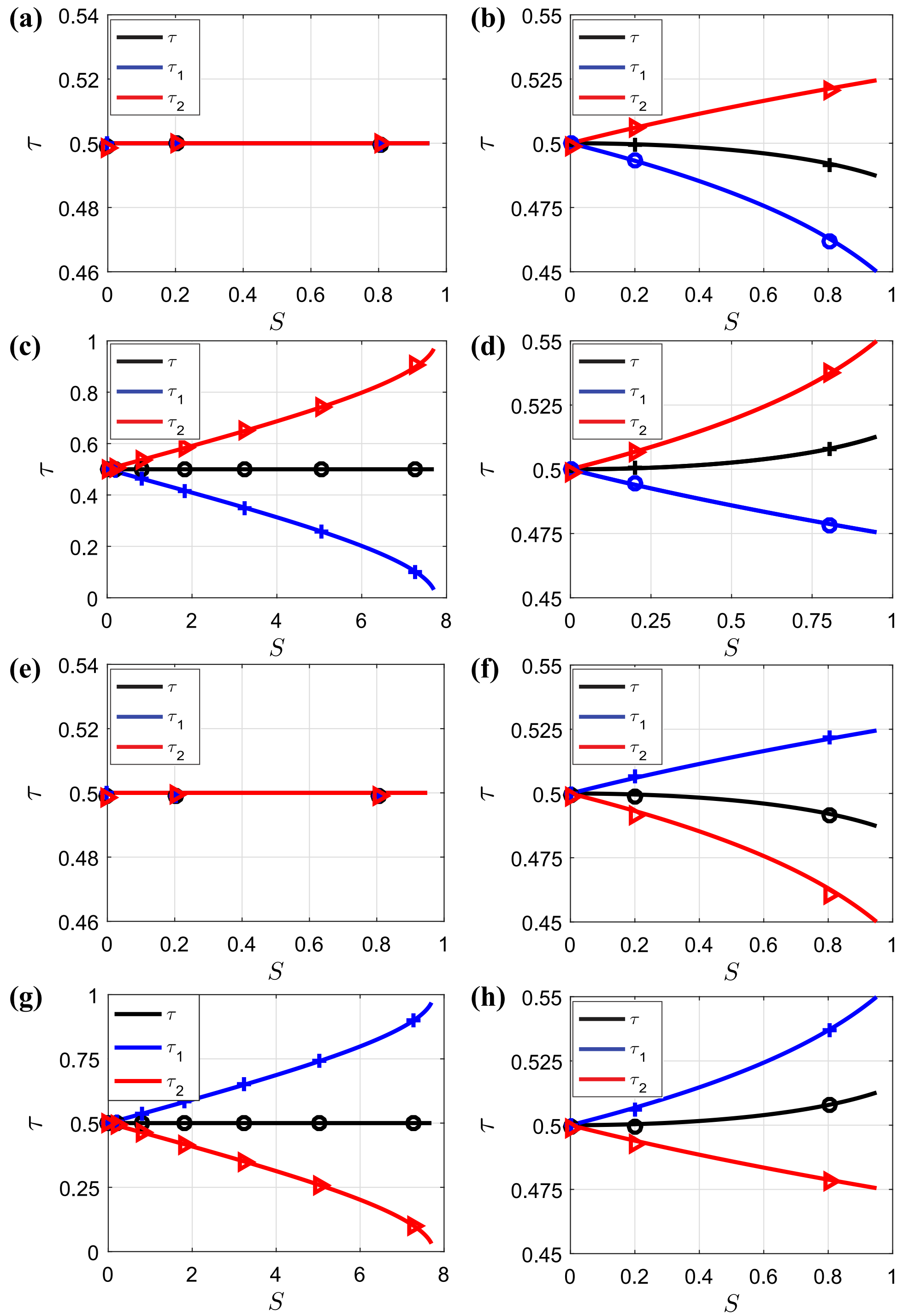

Fig. 8 The dimensionless parameter, τ, varies with the dimensionless magnetic field strength, S, when the magnetic field is applied at $\alpha = 0°$ (**a**), $\alpha = 45°$ (**b**), $\alpha = 90°$ (**c**), $\alpha = 135°$ (**d**), $\alpha = 180°$ (**e**), $\alpha = 225°$ (**f**), $\alpha = 270°$ (**g**) and $\alpha = 315°$ (**h**) for ferromagnetic particle

5 Strong magnetic field

As we explained earlier, the particle could not have a full rotation when the magnetic field strength is increased to a certain value. So, in this section, we will focus on the impeded steady angles of paramagnetic and ferromagnetic particles in the presence of a strong magnetic field.

5.1 Paramagnetic particles

We first examine the rotational dynamics of a paramagnetic particle under a strong magnetic field. Figure 9 shows the evolution of particle orientation angle, ϕ with time, t, and the corresponding impeded angles for different magnetic field strengths and directions. As can be seen, for a fixed magnetic field direction, when the relative strength

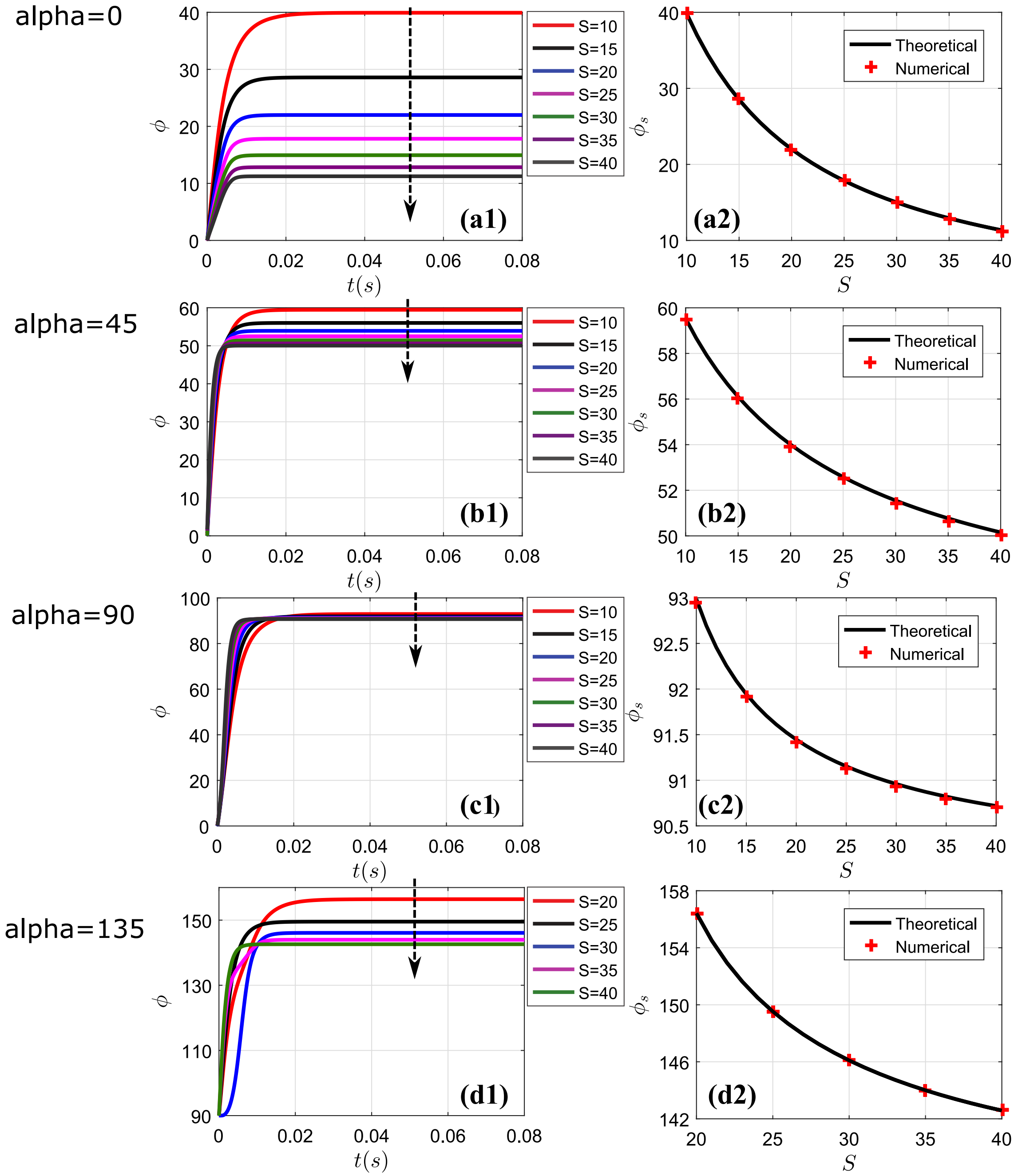

Fig. 9 The time evolution of orientation angle, ϕ, and the stable orientation angle, ϕ_s as a function of S, when the magnetic field is applied at $\alpha = 0°$ (**a**), $\alpha = 45°$ (**b**), $\alpha = 90°$ (**c**) and $\alpha = 135°$ (**d**) for the paramagnetic particle

S is increased, the impeded angle, ϕ_s, is decreased; for a fixed relative strength, when the magnetic field direction is increased, the impeded angle is increased as can be seen in Fig. 9a2, b2, (c2) and (d2). For example, when $S = 30$, $\phi_s = 14.95°$ for $\alpha = 0°$; $\phi_s = 51.43°$ for $\alpha = 45°$; $\phi_s = 90.93°$ for $\alpha = 90°$; $\phi_s = 146.09°$ for $\alpha = 135°$. Recall that S is a parameter to characterize the relative strength between the magnetic and hydrodynamic effects on a magnetic particle. A larger S means the magnetic effect is more pronounced than hydrodynamic effect, and the major axis of the particle becomes more aligned to the magnetic field direction. The theoretical impeded angle, determined from Eq. (17) for S range from 10 to 40 (20–40 for $\alpha = 135°$ due to $S_{cr} = 16$), are shown as solid lines in Fig. 9(a2), (b2), (c2) and (d2). The numerical results of the impeded angles are in close agreement with the theoretical prediction.

5.2 Ferromagnetic particles

Here, we will discuss the rotational dynamics of a ferromagnetic particle ($r_p = 4$) under the strong magnetic field. Figure 10 shows the time evolution of orientation angle, ϕ, and the corresponding impeded angles for different relative strengths and different magnetic field directions. The dependence of ϕ_s on S and α is similar to that of paramagnetic particles. For a fixed magnetic field direction, when the relative strength S is increased, the impeded angle, ϕ_s, is decreased; for a fixed relative strength, when the magnetic field direction is increased, the impeded angle is increased. For example, when $S = 30$, $\phi_s = 25.76°$ for $\alpha = 0°$; $\phi_s = 55.85°$ for $\alpha = 45°$; $\phi_s = 91.82°$ for $\alpha = 90°$; $\phi_s = 163.70°$ for $\alpha = 135°$. The impeded angle, computed from Eq. (17) for S range from 10 to 40, is shown as solid lines in Fig. 10 (a2), (b2), (c2) and (d2), suggesting good agreement between the numerical results and theoretical prediction.

However, compared with the results of paramagnetic particle shown in Fig. 9, the impeded angles of ferromagnetic particles are always larger than those of paramagnetic particles when they are subjected to the same relative strengths (S) and magnetic field direction (α). For example, when

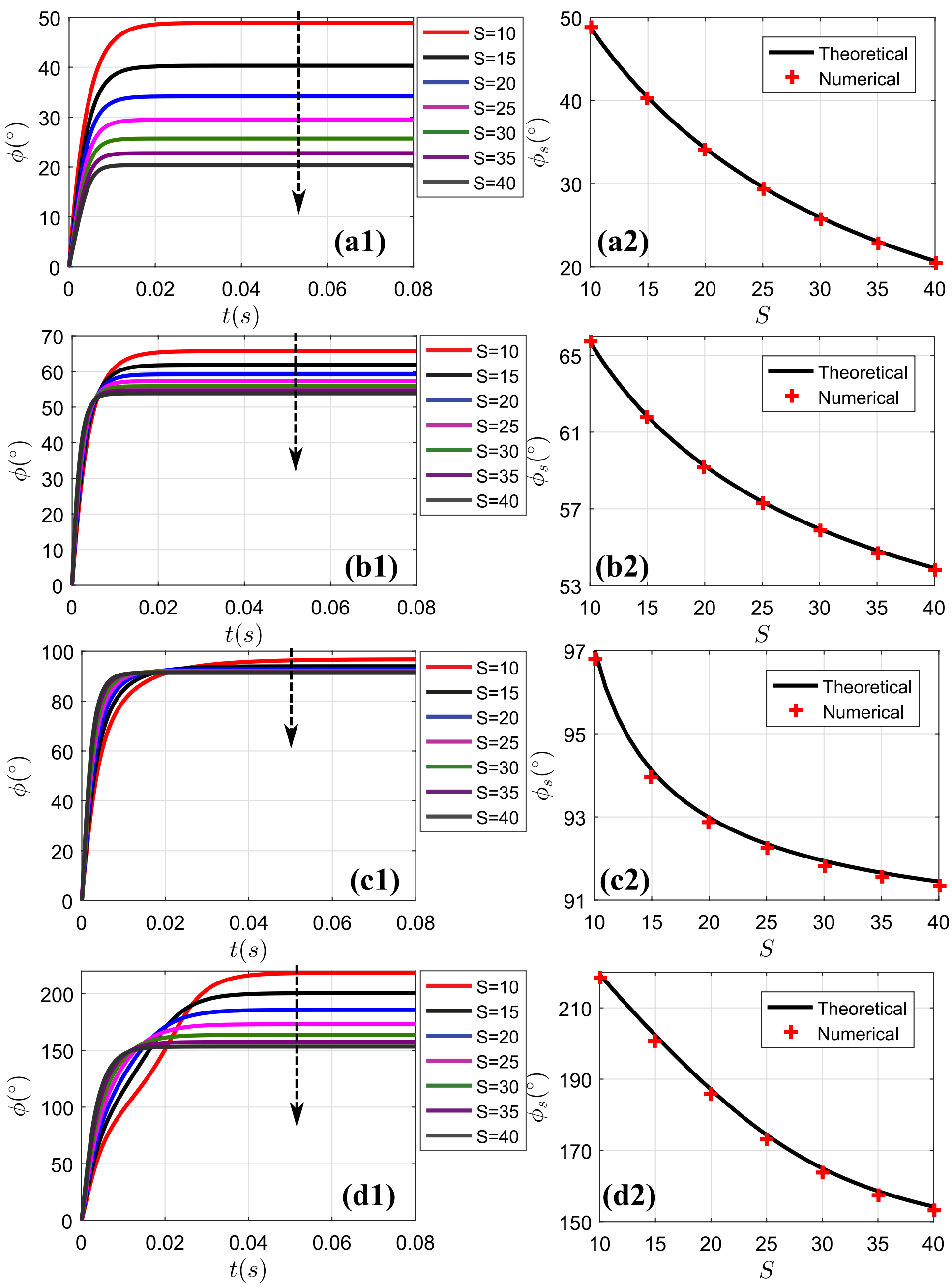

Fig. 10 The time evolution of orientation angle, ϕ, and the stable orientation angle, ϕ_s, as a function of S, when the magnetic field is applied at $\alpha = 0°$ (**a**), $\alpha = 45°$ (**b**), $\alpha = 90°$ (**c**) and $\alpha = 135°$ (**d**) for the ferromagnetic particle

$S = 20$ and $\alpha = 0°$, $\phi_s = 22.00°$ for the paramagnetic particle, while $\phi_s = 34.15°$ for the ferromagnetic particle.

6 Particle lateral migration in a simple shear flow near the wall

The results presented in the previous sections have illustrated many differences of rotational dynamics between paramagnetic and ferromagnetic particles when they are subjected to a uniform magnetic field, where the wall effects can be neglected. Prior investigations have shown lateral migration in wall-bounded shear flows for either paramagnetic particles in a weak magnetic field (Zhou et al. 2017a, b; Zhang and Wang 2018; Cao et al. 2018), or ferromagnetic particles in a strong magnetic field (Matsunaga et al. 2017a, b). However, systemic studies on the lateral migration of paramagnetic and ferromagnetic particles under the weak and strong magnetic fields are absent. Therefore, in this section, we will use numerical simulations to study the lateral migration of the two different particles in a simple shear flow near the wall.

The numerical model of an elliptical particle suspended in a simple shear flow near the wall is shown in Fig. 11a. In this model, the velocity of the bottom wall is kept at zero, while the velocity of the top wall is at a constant velocity $\dot{\gamma} W \mathbf{e}_x$. The length of the channel $L = 900$ µm. The width of the channel W is set to 100 µm. To investigate the effect of the wall, the particle is initially placed at a particle–wall separation distance $y_{p0} = 10$ µm. The effect of the other wall is negligible due to the large separation distance. Our previous numerical study Zhang and Wang (2018) indicated that the inertia effect (Re = 0.125) can cause a small net lateral migration in the absence of magnetic field. Thus, to avoid the inertia effect, the viscosity of the fluid is set to 0.1 Pa·s and the shear rate is set to $\dot{\gamma} = 80\ \mathrm{s}^{-1}$, resulting in a small Reynolds number (Re = 0.008 $\ll$ 1). This way, the effect of magnetic field is isolated to study its influence on particle migration. The other parameters are the same as before.

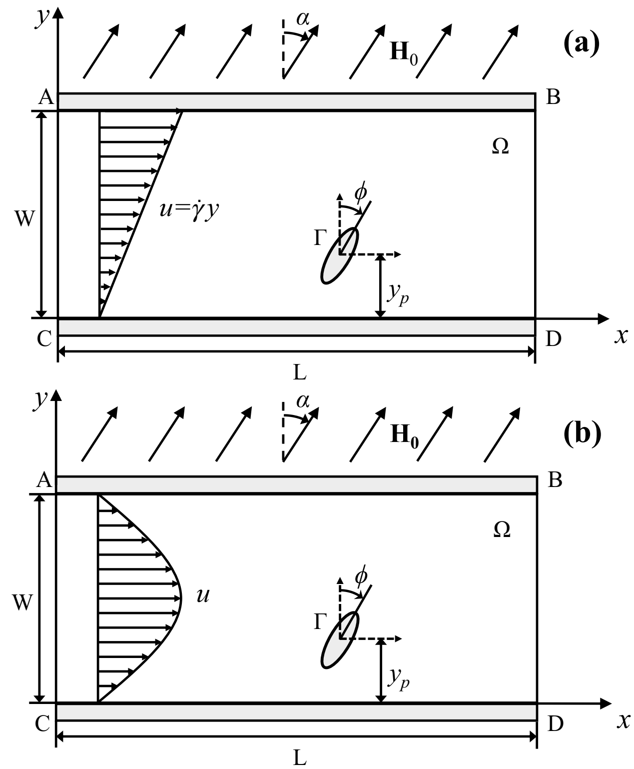

Fig. 11 Schematic illustration of the numerical model of an elliptical particle suspended in a simple shear flow near the wall and in a plane Poiseuille flow in a microchannel under the influence of a uniform magnetic field $\mathbf{H}_0$. The fluid and particle domains are Ω and Γ, respectively. The orientation angle of the particle is denoted by ϕ. The particle–wall separation distance is denoted by y_p

6.1 Weak magnetic field

As we have discussed in Sect. 4, the symmetry property (characterized by τ) of particle's rotational velocity depends on the magnetic properties of the particle, and the direction of the magnetic field. Specifically, for paramagnetic particles, $\tau > 0.5$ when the magnetic field is applied at 0°, and $\tau < 0.5$ for paramagnetic particles when the magnetic field is applied at 90°, while for ferromagnetic particles, $\tau = 0.5$ when the magnetic field is applied at 0°, 90°, 180° and 270°. Second, for paramagnetic particles, $\tau = 0.5$ when the magnetic field is applied at 45° and 135°, while for ferromagnetic particles, $\tau < 0.5$ when the magnetic field is applied at 45° and 225°, and $\tau > 0.5$ when the magnetic field is applied at 135° and 315°. We will discuss those two cases separately to understand their lateral migration.

First, let us discuss about the lateral migration of paramagnetic and ferromagnetic particles when the magnetic field is applied at 0°, 90°, 180° and 270°. Due to a periodicity of $\pi(180°)$ in ϕ for paramagnetic particles, the results for $\alpha = 0°$ and 180°, $\alpha = 90°$ and 270° are the same, so we only need to perform simulations for $\alpha = 0°$ and $\alpha = 90°$. Figure 12 shows that the lateral migration with time over a 2π (or 360°) period for paramagnetic and ferromagnetic particles when the magnetic field of $S = 0.67$ is applied at 0°, 90°, 180° and 270°. As can be seen in Fig. 12a for the paramagnetic particle, the net lateral migration is away from the wall when $\alpha = 0°$, and towards the wall when $\alpha = 90°$. However, for the ferromagnetic particle as shown in Fig. 12b, there are negligible net lateral migrations when the magnetic field is applied at $\alpha = 0°$, 90°, 180° and 270°. Therefore, we can separate paramagnetic and ferromagnetic particles using a simple shear flow near the wall when a weak magnetic field is applied at 0°, 90°, 180° and 270°.

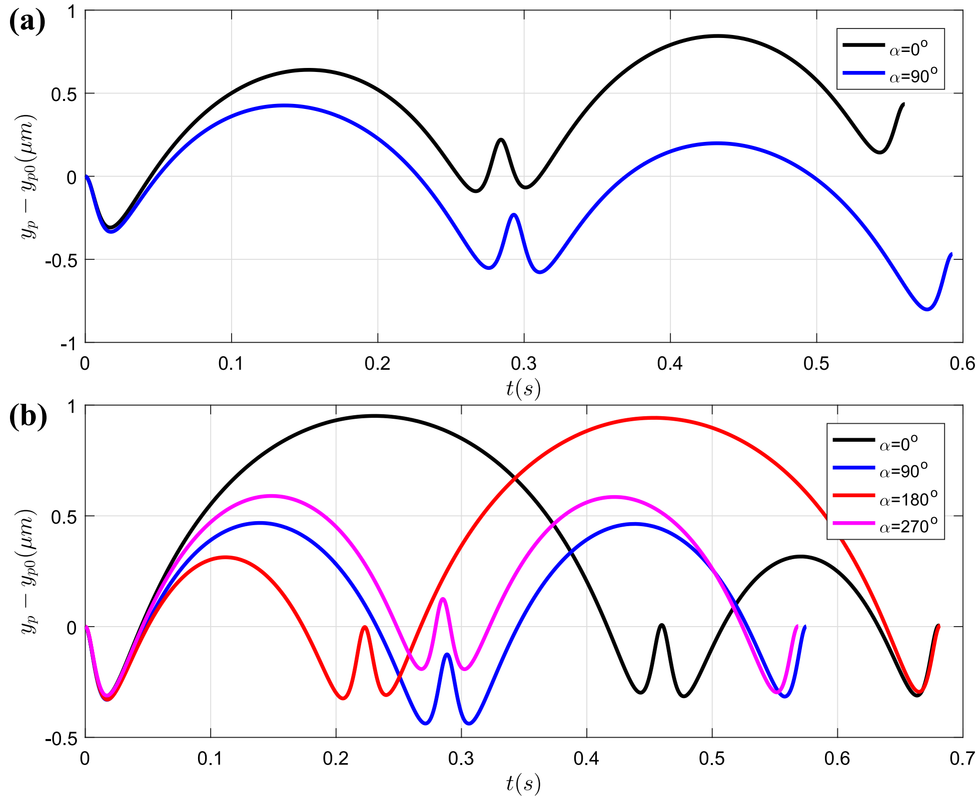

Fig. 12 Transport of the magnetic particles ($r_p = 4$) near the wall under a weak magnetic field. **a** The lateral position of the paramagnetic particle, ($y_p - y_{p0}$), over a period. **b** The lateral position of the ferromagnetic particle, ($y_p - y_{p0}$), over a period

Next, we examine lateral migration of paramagnetic and ferromagnetic particles when $\alpha = 45°, 135°, 225°$ and $315°$. We only carry out simulations when $\alpha = 45°$ and $135°$ for paramagnetic particles. Figure 13 shows that the lateral migration changes with time over a 2π (or $360°$) period for paramagnetic and ferromagnetic particles when a magnetic field of strength $S = 0.67$ is applied at $\alpha = 45°, 135°, 225°$ and $315°$. As can be seen in Fig. 13a, for the paramagnetic particle, there are no net lateral migrations when $\alpha = 45°$, or $135°$. However, for the ferromagnetic particle as shown in Fig. 13b, there is a positive net lateral migration when $\alpha = 135°$ or $225°$, and a negative net lateral migration when the magnetic field is applied at $\alpha = 45°$ and $315°$. Therefore, we can separate the paramagnetic and ferromagnetic particles in a simple shear flow near the wall when the weak magnetic field is applied at $45°, 135°, 225°$ and $315°$. But the net lateral migration over a period is smaller than the first case.

For the paramagnetic particle in a weak magnetic field, our numerical results are consistent with findings of several previous studies (Zhou et al. 2017b; Zhang and Wang 2018; Cao et al. 2018): the particle moves away from the wall when $\tau > 0.5$; the particle moves downwards when $\tau < 0.5$; no net lateral migration when $\tau = 0.5$. This numerical study further confirms same results for the ferromagnetic particle in a weak magnetic field: the particle will move upwards when $\tau > 0.5$; the particle will move downwards when $\tau < 0.5$; no net lateral migration when $\tau = 0.5$.

6.2 Strong magnetic field

As we have discussed in Sect. 5, the impeded angles of the paramagnetic and ferromagnetic particles are different for the same S and α. Thus, we carry out simulations for the paramagnetic and ferromagnetic particles to understand the effect of a strong magnetic field on lateral migration, as shown in Fig. 14. When a strong magnetic field is applied at $\alpha = 0°$, the time evolution of orientation angle ϕ and the lateral migration, ($y_p - y_{p0}$), of paramagnetic (red line) and ferromagnetic (black line) particles are shown in Fig. 14a, b. For both particles, a moderate strength $S = 10$ (solid line) and a large strength $S = 40$ (dash line), the impeded angles and lateral migration are different. But the difference of the impeded angles for $S = 40$ is more significant than those for $S = 10$. The net lateral migration between paramagnetic and ferromagnetic particles also shows marked difference for $S = 40$. This comparison suggests that it would be advantageous to use stronger field strength to separate the paramagnetic and ferromagnetic particles when the magnetic field is applied at $\alpha = 0°$.

Figure 14c, d shows the evolution of orientation angle ϕ and the lateral migration, ($y_p - y_{p0}$), of paramagnetic (red line) and ferromagnetic (black line) particles when a strong magnetic field is applied at $\alpha = 90°$. In this case, there is a larger difference of both impeded angle and lateral migration for $S = 10$ (solid line) than for $S = 40$ (dash

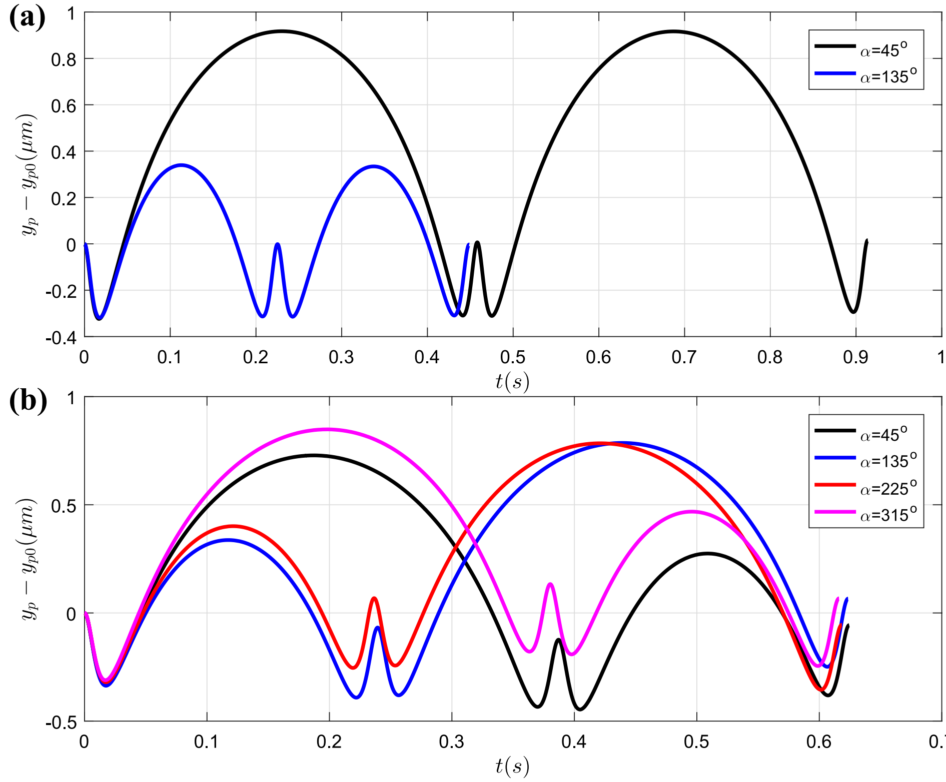

Fig. 13 Transport of the magnetic particles ($r_p = 4$) near the wall under a weak magnetic field. **a** The lateral position of the paramagnetic particle, $(y_p - y_{p0})$, over a period. **b** The lateral position of the ferromagnetic particle, $(y_p - y_{p0})$, over a period

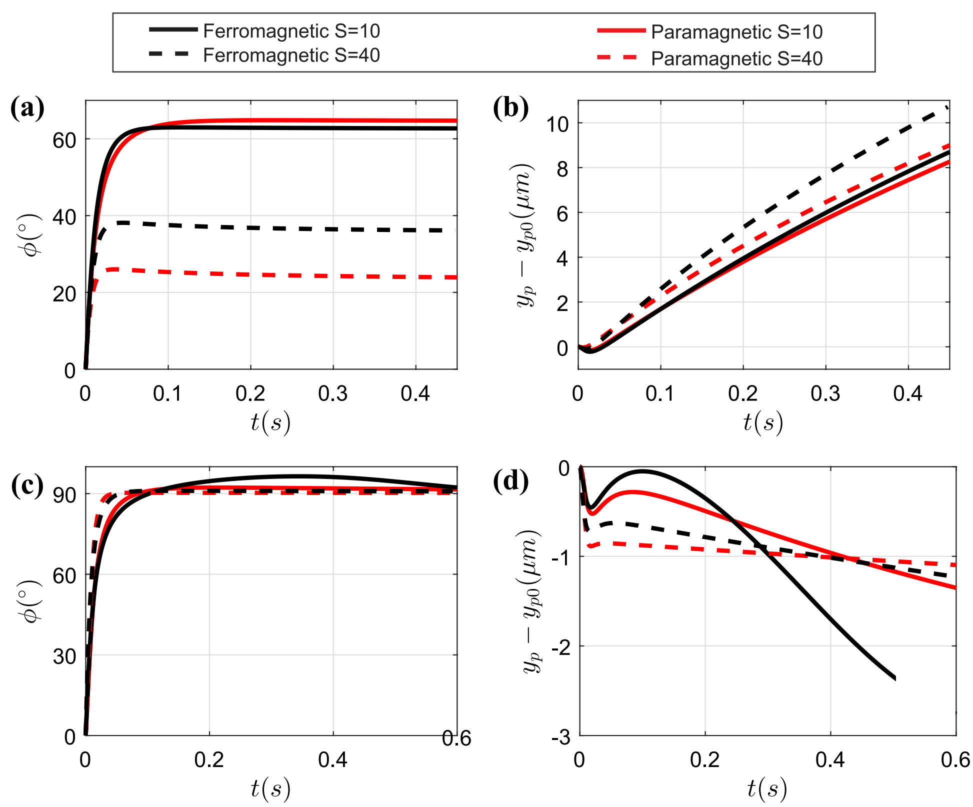

Fig. 14 Transport of the magnetic particle ($r_p = 4$) near the wall under a strong magnetic field. **a** The evolution of orientation angle ϕ and **b** the lateral position of the paramagnetic (red) and ferromagnetic (black) particles $(y_p - y_{p0})$ vary with the time t when the magnetic field is applied at 0°; **c** The evolution of orientation angle ϕ and **d** the lateral migration, $(y_p - y_{p0})$, of paramagnetic(red) and ferromagnetic(black) particles vary with the time t when the magnetic field is applied at 90°

line). This finding suggests that a moderate field strength ($S = 10$) can result in better separation between the paramagnetic and ferromagnetic particles than a stronger field ($S = 40$) if the magnetic field is perpendicular to the flow, i.e., $\alpha = 90°$.

7 Particle lateral migration in a plane Poiseuille flow in a microchannel

While the previous findings are obtained for particles suspended in simple shear flows (constant shear rate), we expect that they are qualitatively valid for Poiseuille flows, which are the predominant form of flow in practical applications. In this section, we study particle lateral migration in a plane Poiseuille flow in a microchannel. The numerical model is shown in Fig. 11b. The width and length of the channel are W = 50 μm and L = 1200μ m, respectively. The initial particle–wall separation distance is $y_{p0} = 12\mu$m. Water is the most commonly used fluid medium, thus we use water as the fluid in this simulation. The average inlet flow velocity is 2.5 mm/s, resulting Reynolds number Re = 0.125.

As we have discussed in Sect. 6, the separation is possible when the magnetic field is applied at 0° and 90°. Here, we perform simulations when the magnetic field is applied at $\alpha = 0°$ and 90°. With a weak magnetic field applied, the particle lateral migration in the plane Poiseuille flow in the microchannel is shown in Fig. 15a, b. As can be seen, the trajectories of paramagnetic particle (red line in Fig. 15) and ferromagnetic particle (black line in Fig. 15) are qualitatively similar to those in a simple shear flow near a wall (Fig. 11b).

When a strong field is used, previous discussions have indicated better separation performance when the magnetic field is applied at $\alpha = 0°$; while for a moderate relative strength (still must be larger than S_{cr}), the field applied at $\alpha = 90°$ leads to a better separation. This finding is confirmed by numerical simulations for $S = 40$ with $\alpha = 0°$ and $S = 12$ with $\alpha = 90°$, as shown in Fig. 15c. Note that the parabolic velocity profile does affect the critical strength, and $S = 12$ is used to impede particle rotation. Nevertheless, the conclusions from simple shear flows apply qualitatively to pressure-driven flows in a channel.

8 Conclusion

In this work, we developed a multi-physics numerical model to investigate the rotational dynamics of paramagnetic and ferromagnetic particles that have elliptical shape, in a simple shear flow and under a uniform magnetic field. We investigated the effects of strength and direction of the magnetic field on rotational dynamics of paramagnetic and ferromagnetic particles. The results show that the symmetry of rotational velocity is modified by the magnetic field. When the magnetic field strength increases to a large enough value (the critical magnetic field strength), the particle rotation is impeded. In a weak field regime (below the critical magnetic field), the particle completes a full rotation, and

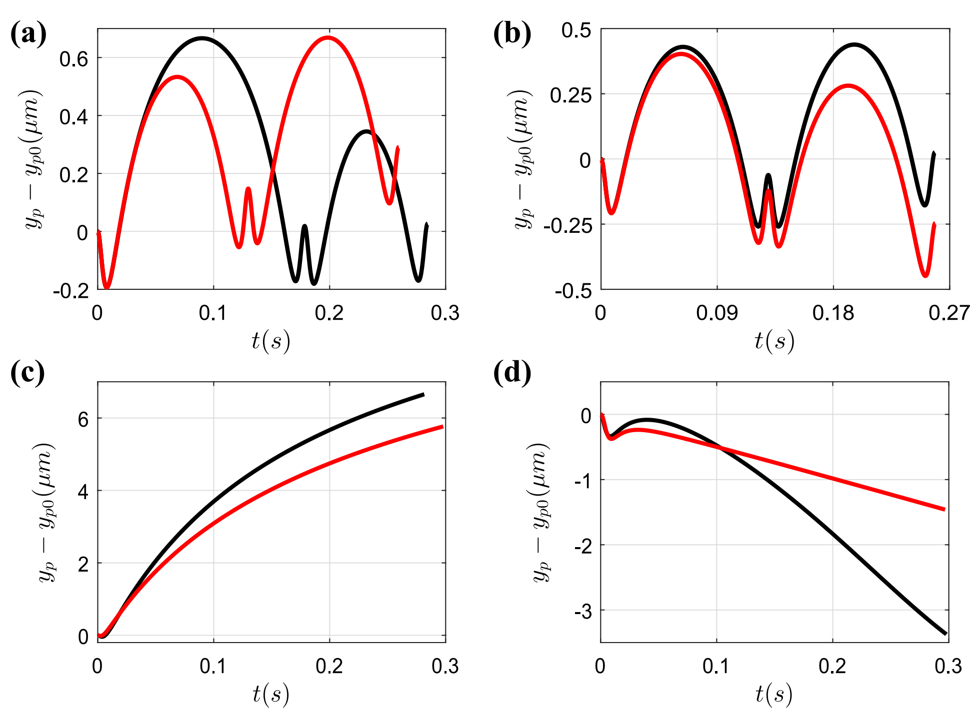

Fig. 15 Transport of the magnetic particle ($r_p = 4$) in a plane Poiseuille flow in a microchannel when the magnetic field is applied at 0° (**a**, **c**) and 90° (**b**, **d**). $S = 0.48$ for (**a**) and (**b**); $S = 40$ for (**c**); $S = 12$ for (**d**). The red line represents for the paramagnetic particle and the black line the ferromagnetic particle

the symmetrical property of particle rotations depends on the direction of the magnetic field. For the same strength and direction of the magnetic field, paramagnetic and ferromagnetic particles exhibit different asymmetric rotational behaviors. In the strong field (above the critical strength), the particles are pinned at their respected steady angles, which depend on the direction of magnetic field. The steady angles of paramagnetic and ferromagnetic particles are different for the same magnetic field strength and direction. The numerical results have very good agreement with that of theoretical analysis.

Based on the findings of the particle rotational dynamics, the lateral migration of paramagnetic and ferromagnetic elliptical particles in a simple shear flow near the wall is investigated. The results show that the paramagnetic and ferromagnetic particles have different lateral migration motions for the same flow and magnetic conditions. Thus, we can separate these two kinds of particles in a simple shear flow under the magnetic field. Finally, the lateral migration of paramagnetic and ferromagnetic particles in a pressure-driven channel flow is investigated. Paramagnetic and ferromagnetic particles in pressure-drive flows behave qualitatively similar to those in simple shear flows, suggesting a useful strategy to manipulate non-spherical micro-particles in the microfluidic devices.

References

Ai Y, Qian S (2010) Dc dielectrophoretic particle-particle interactions and their relative motions. J Colloid Interface Sci 346(2):448–454

Ai Y, Beskok A, Gauthier DT, Joo SW, Qian S (2009a) Dc electrokinetic transport of cylindrical cells in straight microchannels. Biomicrofluidics 3(4):044110

Ai Y, Joo SW, Jiang Y, Xuan X, Qian S (2009b) Pressure-driven transport of particles through a converging-diverging microchannel. Biomicrofluidics 3(2):022404

Ai Y, Zeng Z, Qian S (2014) Direct numerical simulation of ac dielectrophoretic particle-particle interactive motions. J Colloid Interface Sci 417:72–79

Allan R, Mason S (1962) Particle behaviour in shear and electric fields. ii. Rigid rods and spherical doublets. Proc R Soc Lond A Math Phys Eng Sci 267(1328):62–76

Bucak S, Sharpe S, Kuhn S, Hatton TA (2011) Cell clarification and size separation using continuous countercurrent magnetophoresis. Biotechnol Prog 27(3):744–750

Cao Q, Li Z, Wang Z, Han X (2018) Rotational motion and lateral migration of an elliptical magnetic particle in a microchannel under a uniform magnetic field. Microfluid Nanofluid 22(1):3

Chaffey C, Mason S (1964) Particle behavior in shear and electric fields. III. rigid spheroids and discs. J Colloid Sci 19(6):525–548

Chen P, Huang YY, Hoshino K, Zhang JX (2015) Microscale magnetic field modulation for enhanced capture and distribution of rare circulating tumor cells. Sci Rep 5:8745

Gavze E, Shapiro M (1997) Particles in a shear flow near a solid wall: effect of nonsphericity on forces and velocities. Int J Multiph Flow 23(1):155–182

Gijs MA (2004) Magnetic bead handling on-chip: new opportunities for analytical applications. Microfluid Nanofluid 1(1):22–40

Gijs MA, Lacharme F, Lehmann U (2009) Microfluidic applications of magnetic particles for biological analysis and catalysis. Chem Rev 110(3):1518–1563

Hu HH, Patankar NA, Zhu M (2001) Direct numerical simulations of fluid-solid systems using the arbitrary Lagrangian-Eulerian technique. J Comput Phys 169(2):427–462

Jeffery GB (1922) The motion of ellipsoidal particles immersed in a viscous fluid. Proc R Soc Lond A Math Phys Eng Sci 102(715):161–179

Leal L (1980) Particle motions in a viscous fluid. Annu Rev Fluid Mech 12(1):435–476

Matsunaga D, Meng F, Zöttl A, Golestanian R, Yeomans JM (2017a) Focusing and sorting of ellipsoidal magnetic particles in microchannels. Phys Rev Lett 119:198002. https://doi.org/10.1103/PhysRevLett.119.198002

Matsunaga D, Zöttl A, Meng F, Golestanian R, Yeomans JM (2017b) Far-field theory for trajectories of magnetic ellipsoids in rectangular and circular channels. arXiv:171100376

Okagawa A, Cox R, Mason S (1974) Particle behavior in shear and electric fields. VI. the microrheology of rigid spheroids. J Colloid Interface Sci 47(2):536–567

Pamme N (2006) Magnetism and microfluidics. Lab Chip 6(1):24–38

Pamme N (2012) On-chip bioanalysis with magnetic particles. Curr Opin Chem Biol 16(3–4):436–443

Pankhurst QA, Connolly J, Jones S, Dobson J (2003) Applications of magnetic nanoparticles in biomedicine. J Phys D Appl Phys 36(13):R167

Shine A, Armstrong R (1987) The rotation of a suspended axisymmetric ellipsoid in a magnetic field. Rheol Acta 26(2):152–161

Sobecki CA, Zhang J, Zhang Y, Wang C (2018) Rotational dynamics of paramagnetic and ferromagnetic ellipsoidal particles in a simple shear flow. Submitted (2)

Stratton JA (2007) Electromagnetic theory. John Wiley & Sons, New Jersey

Suwa M, Watarai H (2011) Magnetoanalysis of micro/nanoparticles: A review. Anal Chim Acta 690(2):137–147

Winkleman A, Perez-Castillejos R, Gudiksen KL, Phillips ST, Prentiss M, Whitesides GM (2007) Density-based diamagnetic separation: devices for detecting binding events and for collecting unlabeled diamagnetic particles in paramagnetic solutions. Anal Chem 79(17):6542–6550

Zborowski M, Sun L, Moore LR, Williams PS, Chalmers JJ (1999) Continuous cell separation using novel magnetic quadrupole flow sorter. J Magn Magn Mater 194(1–3):224–230

Zhang J, Wang C (2018) Numerical study of lateral migration of elliptical magnetic microparticles in microchannels in uniform magnetic fields. Magnetochemistry 4(1):16

Zhou R, Bai F, Wang C (2017a) Magnetic separation of microparticles by shape. Lab Chip 17(3):401–406

Zhou R, Sobecki CA, Zhang J, Zhang Y, Wang C (2017b) Magnetic control of lateral migration of ellipsoidal microparticles in microscale flows. Phy Rev Appl 8(2):024019

Zhou Y, Xuan X (2016) Diamagnetic particle separation by shape in ferrofluids. Appl Phys Lett 109(10):102405

Zhou Y, Song L, Yu L, Xuan X (2016) Continuous-flow sheathless diamagnetic particle separation in ferrofluids. J Magn Magn Mater 412:114–122